Direct aperture optimization: A turnkey solution for step-and-shoot IMRT

D. M. Shepard, M. A. Earl, X. A. Li, S. Naqvi, and C. Yu
University of Maryland School of Medicine, Department of Radiation Oncology, 22 South Greene St., Baltimore, Maryland 21201-1595

(Received 26 September 2001; accepted for publication 12 March 2002; published 13 May 2002)

IMRT treatment plans for step-and-shoot delivery have traditionally been produced through the optimization of intensity distributions (or maps) for each beam angle. The optimization step is followed by the application of a leaf-sequencing algorithm that translates each intensity map into a set of deliverable aperture shapes. In this article, we introduce an automated planning system in which we bypass the traditional intensity optimization, and instead directly optimize the shapes and the weights of the apertures. We call this approach ''direct aperture optimization.'' This technique allows the user to specify the maximum number of apertures per beam direction, and hence provides significant control over the complexity of the treatment delivery. This is possible because the machine dependent delivery constraints imposed by the MLC are enforced within the aperture optimization algorithm rather than in a separate leaf-sequencing step. The leaf settings and the aperture intensities are optimized simultaneously using a simulated annealing algorithm. We have tested direct aperture optimization on a variety of patient cases using the EGS4/BEAM Monte Carlo package for our dose calculation engine. The results demonstrate that direct aperture optimization can produce highly conformal step-and-shoot treatment plans using only three to five apertures per beam direction. As compared with traditional optimization strategies, our studies demonstrate that direct aperture optimization can result in a significant reduction in both the number of beam segments and the number of monitor units. Direct aperture optimization therefore produces highly efficient treatment deliveries that maintain the full dosimetric benefits of IMRT. [DOI: 10.1118/1.1477415]

Key words: IMRT, inverse treatment planning, optimization, intensity modulation

I. INTRODUCTION

Current inverse-planning algorithms for step-and-shoot IMRT[1–7] typically divide the beam's eye view of the tumor into a series of finite size pencil beams. The pencil beam dose distributions are computed and their corresponding weights are optimized. During the optimization, the quality of the plan is scored based on the predefined treatment goals. After the optimization is complete, a leaf-sequencing algorithm translates the final intensity maps for each beam direction into a set of deliverable beam segments. This strategy is illustrated in Figs. 1 and 2. A general rule of thumb is that for each beam angle, the number of segments that are required is two to three times the number of levels in the intensity map.[7] This number, however, is dependent upon the specific inverse planning algorithm and the multileaf collimator (MLC) design.

Current algorithms typically ignore the constraints imposed by the MLC during the intensity optimization. These constraints are only accounted for in the leaf-sequencing step. Consequently, the resulting MLC leaf sequence often contains a large number of segments resulting in a large monitor unit-to-cGy ratio. The large number of segments also creates significant uncertainties in leakage, head scatter, and tongue-and-groove effects.

In this article, we present a new inverse planning technique called direct aperture optimization (DAO). With this technique, all of the constraints imposed by the MLC are included in the optimization, thereby eliminating the need for a separate leaf-sequencing step. A key feature of this approach is that the user specifies the number of segments to be delivered as a constraint in the optimization. DAO is designed to maintain the simplicity and the efficiency of conventional radiation therapy while providing the dosimetric benefits offered by IMRT.

Researchers have previously investigated the idea of eliminating leaf sequencing by incorporating MLC constraints into inverse planning. Tervo[8] proposed a technique for including MLC constraints into a feasibility algorithm. Tervo's algorithm maintains the feasibility of the MLC shapes while it searches for a plan that meets the prescribed dosimetric constraints. De Gersem *et al.*[9] have implemented a constructive heuristic[10] that loops over a series deterministic leaf-position changes. The heuristic operates in a greedy fashion whereby it accepts every leaf-position change that improves the objective function and rejects all changes that make the objective function worse. Any change resulting in an infeasible MLC shape is rejected. In De Gersem's algorithm, the beam weights are optimized separately from the MLC positions. Our algorithm differs from these implementations in that a global optimization routine is applied. Also, the leaf positions and aperture weights are optimized simultaneously. Another key feature of DAO is that it does not rely on the use of a segmentation routine to select the initial leaf positions. Rather, the leaf positions are initialized to match the beam's eye view of the target.

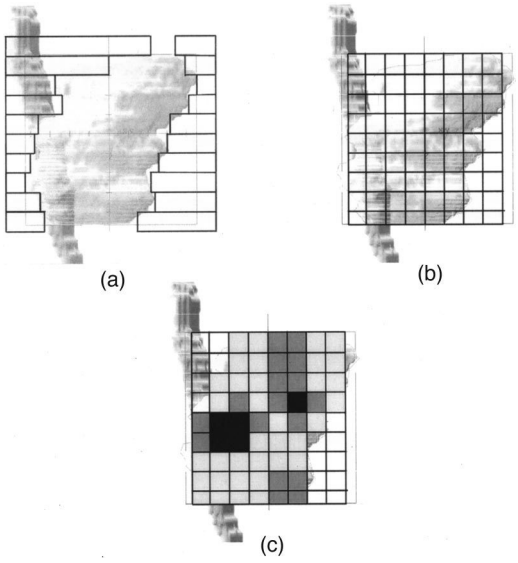

FIG. 1. An illustration of the conventional inverse planning approach. (a) The leaves of the MLC are shaped to match the beam's eye view (BEV) of the tumor volume. (b) The BEV of the tumor is divided into a series of finite size pencil beams, and the corresponding pencil beam dose distributions are computed. (c) The pencil beam intensities are optimized and the result is an optimized intensity map. The three shades in the map represent three different intensity levels. Before delivery, this intensity map must be translated into deliverable shapes.

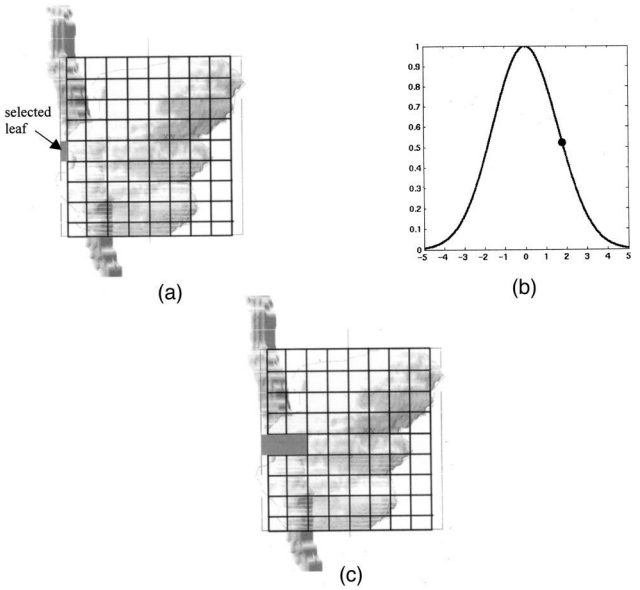

FIG. 3. The direct aperture optimization routine randomly selects a leaf position for modification. (a) The highlighted leaf has been chosen by the optimizer. (b) A random number is selected on a Gaussian to determine the size and direction of the change in leaf position. In this case, the leaf will move into the field by 2 units (2 pencil beam widths).

II. MATERIALS AND METHODS

A. Optimization of the aperture shapes and aperture intensities

The DAO algorithm takes as input the (*i*) beam angles, (*ii*) beam energies, and (*iii*) number of apertures per beam angle. Each aperture is initialized to the beam's eye view of the target. The optimization begins by computing the objective function for the initial beam configuration (see Sec. II C for objective function details). The algorithm then cycles through all of the variables, which are to be optimized. These variables are (*i*) the leaf positions for each aperture and (*ii*) the weight assigned to each aperture. After the optimizer selects a particular variable, a change of random size is sampled from a Gaussian distribution. The width of the Gaussian decreases according to the schedule

$$\sigma = 1 + (A-1)e^{-\log(n_{\text{succ}}+1)/T_0^{\text{step}}}, \tag{1}$$

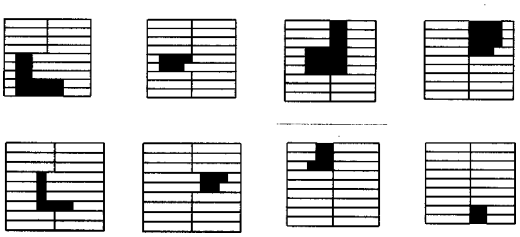

FIG. 2. A leaf sequencing algorithm was applied to the intensity map in Fig. 1(c). The leaf sequencer determined that the optimized intensity pattern with three intensity levels can be delivered with these eight apertures.

where A is the initial width, n_{succ} is the number of successful iterations, and T_0^{step} quantifies the rate of cooling[11,12] (see Fig. 3). A change in leaf position is rejected if the new aperture shape violates any of the constraints imposed by the multileaf collimator. Otherwise, the change is applied, the new dose distribution is computed, and the corresponding objective function value is determined. The change is accepted if the value of the objective function decreases. If the objective function value increases, the change is accepted with a probability P given by a standard Boltzmann simulated annealing cooling schedule[13–15]

$$P = 2B\frac{1}{1+e^{\log(n_{\text{succ}}+1)/T_0^{\text{prob}}}}, \tag{2}$$

where B is the initial probability and T_0^{prob} quantifies the rate of cooling. The number of successes, n_{succ}, in Eqs. (1) and (2) is incremented if a change results in either a decrease in the objective function value or an increase in the objective function value that passes the probability constraint. Prior to optimization, the user specifies n_{succmax}, the value of n_{succ} at which the optimization procedure terminates.

Prior to evaluation of the objective function, each new aperture shape is tested for deliverability. In other words, the optimizer incorporates the MLC constraints. Hence, no separate leaf sequencing is required. For example, our Elekta SL20 collimator enforces a minimum separation of 0.8 cm between each leaf and its opposing leaf. The separation requirement applies to each leaf and the leaves adjacent to its opposing leaf,[16,17] thus making interdigitation impossible. The leaves also have a limit of travel across the central axis of 12.5 cm. The algorithm can be easily modified to incorporate the constraints specific to any other collimator type.

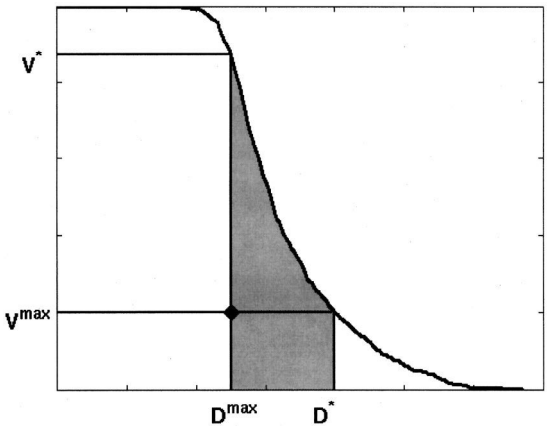

FIG. 4. An illustration of a DVH based penalty that is used to guide the optimization. The voxels shaded in gray are penalized in order to drive the optimizer to meet the DVH specification that is indicated by the black diamond.

A beneficial feature of DAO is that one can include a constraint on the minimum size for each aperture. For example, one might choose to reject any change in leaf position that results in an aperture with an open area of less than 4 cm^2. One can also place a lower bound on the weight assigned to each aperture. This lower bound might be used to disallow apertures that deliver fewer than two monitor units.

B. Defining the treatment goals

The treatment goals are defined using a cumulative dose volume histogram (DVH). The user specifies a minimum and a maximum dose for the tumor volume. For each sensitive structure, the user can specify the maximum dose allowed, a tolerance dose, and additional dose volume constraints. A dose volume constraint is defined using a point on the DVH that indicates both a dose limit ($D^{\max}$) and a fraction of the sensitive structure ($V^{\max}$) that is permitted to exceed that limit. The relative importance of each goal is input by the user as a numerical weight.

C. Objective function

The objective function reduces the entire treatment plan into a single numerical value that is to be minimized. For the results shown in this article, a weighted least squared objective function was used. In its most basic form the objective function is given by

$$\min_{m\geqslant 0}\sum_{m}\ \theta_m\sum_{i\in m}\ (d_i^d-d_i^p)^2, \tag{3}$$

where m is the structure index, θ_m is the structure weight, and i is the voxel index. For the voxels located in the target, d_i^p is the prescribed dose. d_i^p represents a tolerance dose for all voxels located in a sensitive structure or in the normal tissue. For our simulations, the weighting factor assigned to each region of interest is normalized to the number of voxels in the region of interest. This prevents a large structure from dominating the optimization. In the optimization, the objective function is reevaluated after each change in either a leaf position or an aperture weight. If, however, a change in leaf position violates a MLC constraint, the change is immediately rejected without a reevaluating of the objective function.

We improve the flexibility of the objective function by allowing separate penalties for underdosage and overdosage. Additional flexibility is provided by allowing dose volume constraints of the form "no more than x percent of this sensitive structure can exceed a dose of y." For this type of constraint, the user specifies both a dose limit and a fraction of the structure that can exceed the dose limit. Within the context of our least squares objective function, DVH constraints are applied using a technique first described by Börtfeld *et al.*[18] for a gradient-based optimization algorithm and extended to an iterative format by Shepard *et al.*[19,20] For each dose volume constraint, a penalty is only applied to a select subset of the voxels in the sensitive structure. A voxel in the sensitive structure is penalized if it receives a dose between $D^{\max}$ and D^* where D^* is the current dose at which $V^{\max}$ is exceeded on the cumulative dose volume histogram (see Fig. 4). The voxels that are penalized are those voxels that receive the smallest excess dose above $D^{\max}$. These particular voxels are penalized because they require the smallest reduction in dose in order to satisfy the DVH specification. By penalizing these voxels, one has the greatest chance of realizing a dose reduction without a significant loss of dose

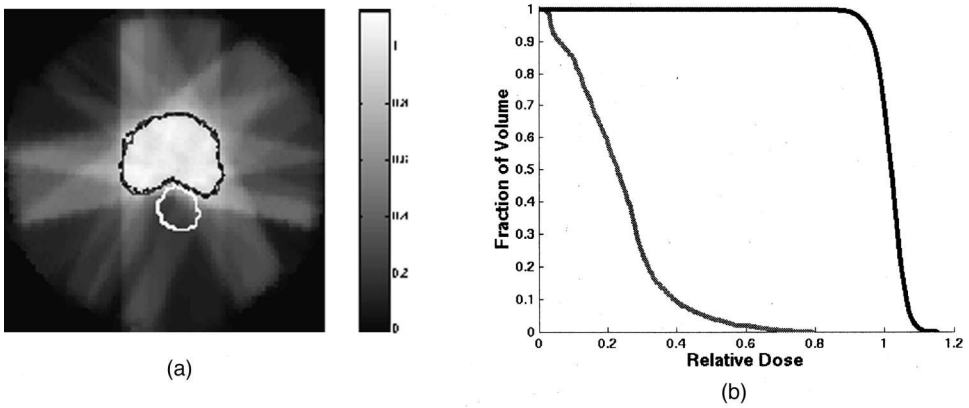

(a) (b)

FIG. 5. (a) An optimized dose distribution produced by direct aperture optimization. The tumor volume is outlined in gray with the 90% isodose line show, as a black dashed line. The sensitive structure is outlined in white. Note the conformity of the 90% isodose line. (b) The corresponding DVH.

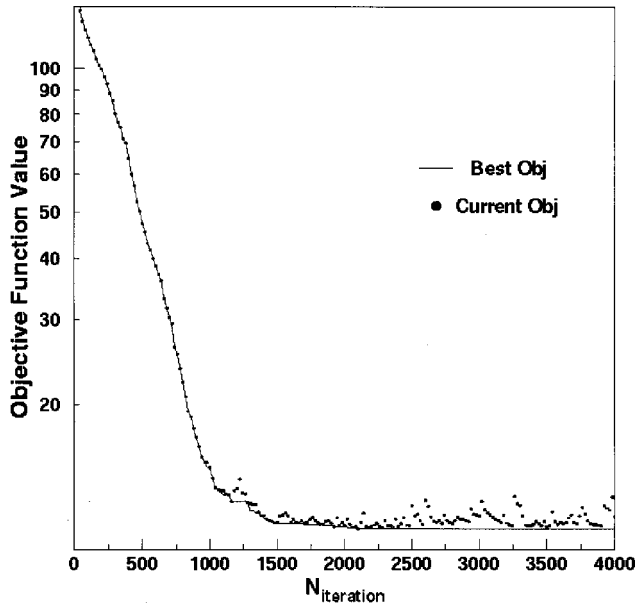

FIG. 6. A plot of the best objective function vs iteration. Note that with simulated annealing the current objective function both increases and decreases during the optimization.

uniformity in the tumor. It should be noted that the subset of penalized voxels changes with each iteration.

D. Monte Carlo dose calculation

We have used the EGS4/BEAM[21] Monte Carlo system as our dose calculation engine. The BEAM code was used to simulate an Elekta SL20 linac equipped with a MLC. Another EGS4 user code, DOSXYZ, was employed to obtain 3-D dose distributions on phantoms and on CT images. The BEAM code outputs the phase-space data, which include all the particle information (i.e., the charge, position, direction, energy, and history tag for each particle). These phase-space data are then used as the input to the dose calculation. The linac simulation was performed in two steps. First, the components above the MLC (including target, primary collimator, flattening filters, ion chambers, and mirror) were simulated. The remaining components (MLC, diaphragms, and air gap) were then simulated starting with the phase space files scored in the first step on a plane immediately above MLC. For our SL20 linac, the first simulation only needed to be performed once. The later simulation was carried out for a series of rectangular field shapes and for any field apertures generated by the direct aperture optimization routine. The entire Monte Carlo process has previously been validated.[22]

The pencil beam dose distributions are computed before the optimization using the DOSXYZ code with a rectangular MLC shape large enough to cover the BEV of the target plus a margin. These pencil beams are generated at the predetermined beam angles. The total dose from each aperture is computed as a sum of all of the unblocked pencil beams. Each field shape undergoes hundreds of modifications during the optimization. After each change in leaf position, the affected pencil beams are simply added or subtracted from the total dose distribution. This dose calculation can thus be performed very rapidly. At the end of the optimization, a final

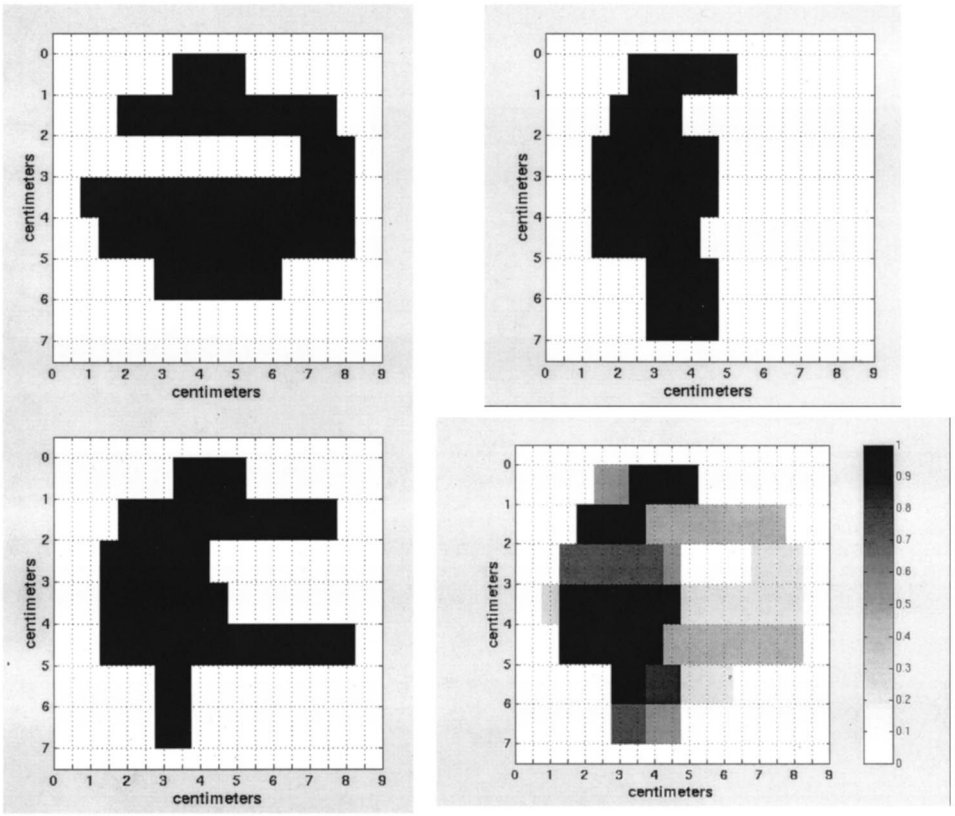

FIG. 7. The three aperture shapes and corresponding intensity map for one beam direction. The open area of each aperture is shown in black.

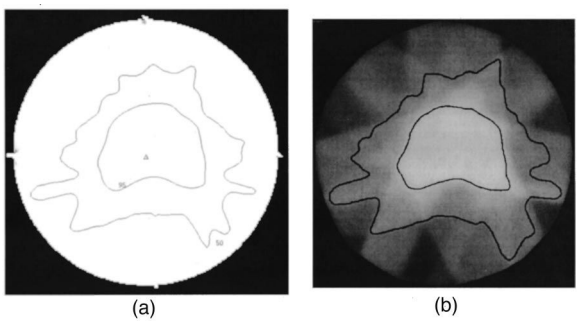

FIG. 8. (a) A predicted dose distribution for direct aperture optimization using seven beam angles with three apertures for each. The inner line is the 95% isodose line while the outer line is the 50% isodose line. (b) The measured dose distribution as determined from a scanned film after delivery to the cylindrical phantom. The 95% and 50% isodose lines are shown.

dose calculation is performed using the optimized apertures and aperture weights.

Several computer programs were developed to automate the entire Monte Carlo process. These programs include (*i*) the conversion of actual beam setup coordinate system (e.g., isocenter coordinates, angles of gantry, collimator and couch) of the linac to the coordinate system for the Monte Carlo calculation, (*ii*) the generation of Monte Carlo input files for all pencil beams, and (*iii*) the translation of leaf positions produced by the DAO algorithm into a format suitable for the BEAM code. The Monte Carlo calculation of the pencil beams was run in parallel on 12 Pentium III 750 MHz PCs. The computation time required to generate pencil beams ranges from 2 to 6 h depending on the number of beams and their field sizes.

E. Number of intensity levels

With DAO, the intensity of each aperture is allowed to vary continuously. In combination, these apertures produce complex intensity maps. The relationship between the number of intensity levels per beam direction and the number of apertures per beam direction can be expressed as

$$N_n = 2^n - 1, \tag{4}$$

where n is the number of apertures and N is the possible number of intensity levels. It is thus possible to have seven intensity levels when just three apertures are used. With five apertures, the number of possible intensity levels jumps to 31. Sixty-three intensity levels are possible when six apertures are used. Consequently, highly modulated intensity patterns can be produced using a small number of apertures per beam direction. This offers a significant advantage over the traditional two-step process where the number of apertures is typically two to three times the number of intensity levels.[7] For instance, for 15 intensity levels, DAO requires 4 apertures as compared to the 30 to 45 apertures required by traditional algorithms.

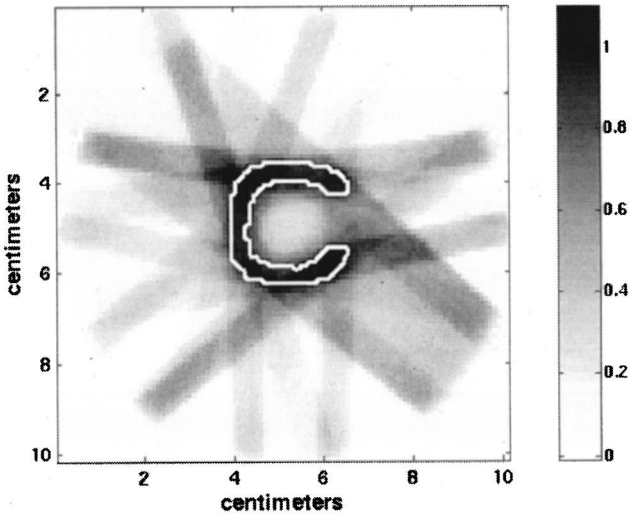

FIG. 9. An optimized dose distribution for a c-shaped target with a centrally located sensitive structure. In this case seven beams angles were used with seven apertures per beam direction. The target is outlined in white.

TABLE I. The objective function and corresponding optimization time for the C-shaped target run with 1, 3, 5, 7, and 9 apertures per beam angle. Note that as the number apertures per beam angle increases there is a corresponding improvement in the objective function value.

No. of apertures	Objective function	Optimization time (min)
1	56.82	0.92
3	22.04	3.42
5	15.66	6.02
7	14.30	12.20
9	11.48	18.15

F. Phantom studies

Initial tests of the DAO algorithm were performed on a cylindrical phantom. Results are presented for a concave target with an adjacent sensitive structure. Seven equispaced beam angles were used with three apertures shapes per angle. Each pencil beam projected to 1.0 cm by 0.5 cm at isocenter. The voxel size was 0.2 cm by 0.2 cm by 0.5 cm. The optimization included 5691 voxels in the target, 1952 voxels in the sensitive structure, and 7567 normal tissue voxels. A total of 441 variables were included in the optimization (10 leaf pairs $\times$ 2 leafs per pair $\times$ 7 angles $\times$ 3 apertures per angle $+$ 21 aperture weights).

For a C-shaped target, optimizations were run using 1, 3, 5, 7, and 9 apertures per beam direction. This test was designed to examine the extent to which the quality of the dose distribution is related to the number of apertures per beam direction. The pencil beam size was 1.0 cm by 0.5 cm projected to the isocenter, and a total of 12 702 voxels were included in the optimization.

G. Prostate patient

Additional tests were performed on a prostate patient. Seven equispaced beam angles were used with three apertures per angle. A pencil beam size of 1 cm by 0.5 cm was used with a total of 24 735 voxels included in the optimiza-

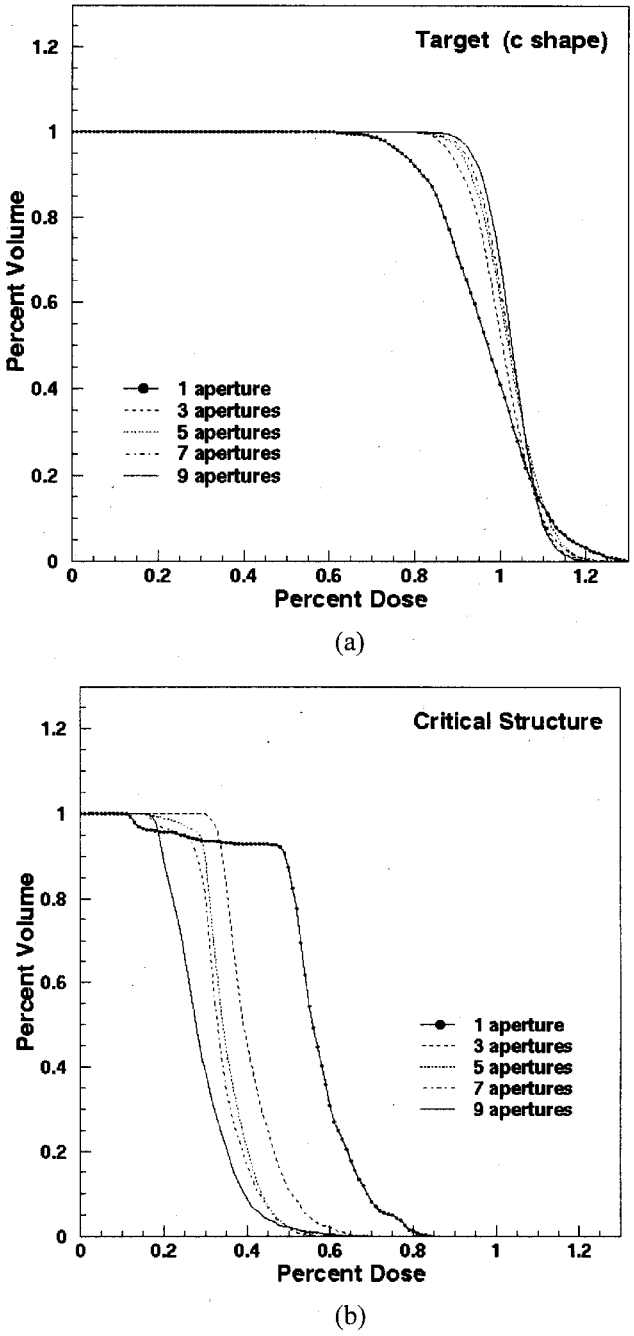

FIG. 10. Dose volume histogram plots for the c-shape target run using 1, 3, 5, 7, and 9 apertures per beam direction. (a) DVH for the target. Note that the target dose uniformity improves with each increase in the number of apertures. (b) DVH for the centrally located critical structure. Note that the dose to the critical structure is reduced with each increase in the number of apertures.

tion. The voxel size was 0.4 cm by 0.4 cm by 0.3 cm. The sensitive structures in this case included the rectum and bladder.

H. Head and neck patient

Results are shown for a head and neck case. In this case seven beam angles were used with three apertures per beam angle. The sensitive structures included the eyes, the optic

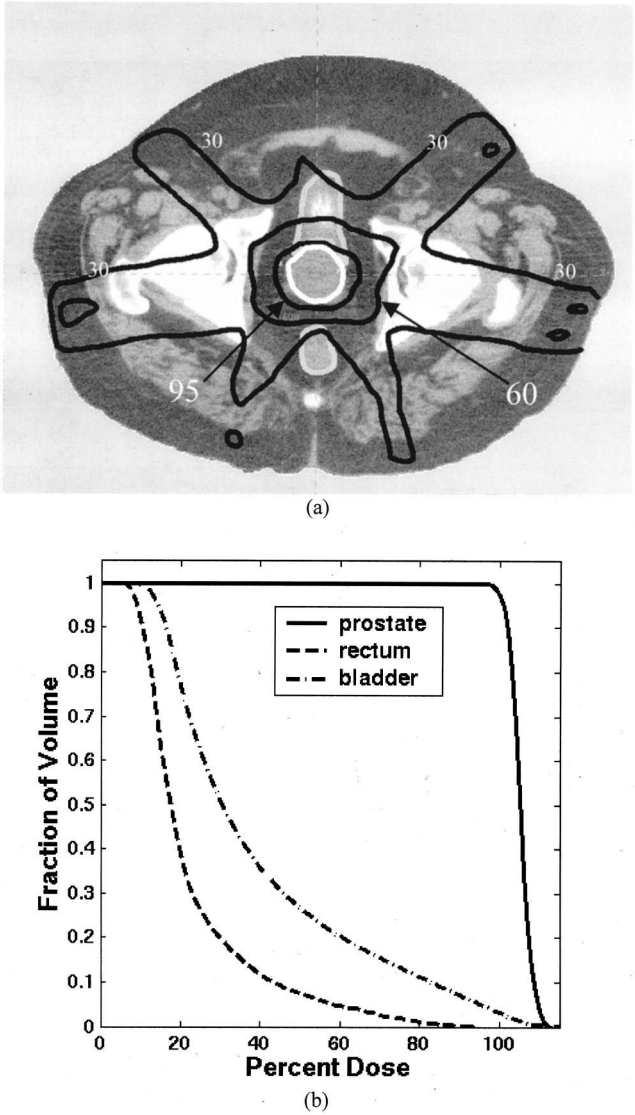

FIG. 11. Optimized treatment plan and corresponding DVH for a patient with prostate cancer using seven equispaced beam angles and three apertures per beam direction. The 95%, 60%, and 30% isodose lines are shown.

nerves, the spinal cord, and the brain stem. Each pencil beam projected to 1 cm by 0.5 cm at isocenter. A voxel size of 0.3 cm by 0.3 cm by 0.3 cm was used and a total of 22 255 voxels were scored during the optimization.

I. Consistency test

A key advantage of the use of a stochastic optimization approach such as simulated annealing is the ability to avoid local minima. In practice, however, the avoidance of local minima is dependent upon the annealing schedule, the choice of initial temperature, the number of iterations performed at each temperature, and how much the temperature is decremented at each step as the cooling proceeds. Consequently, one must balance the need for a short optimization time with the desire to avoid local minima. To address this issue, we present results obtained for the head and neck patient using 100 different random number seeds. Our standard cooling

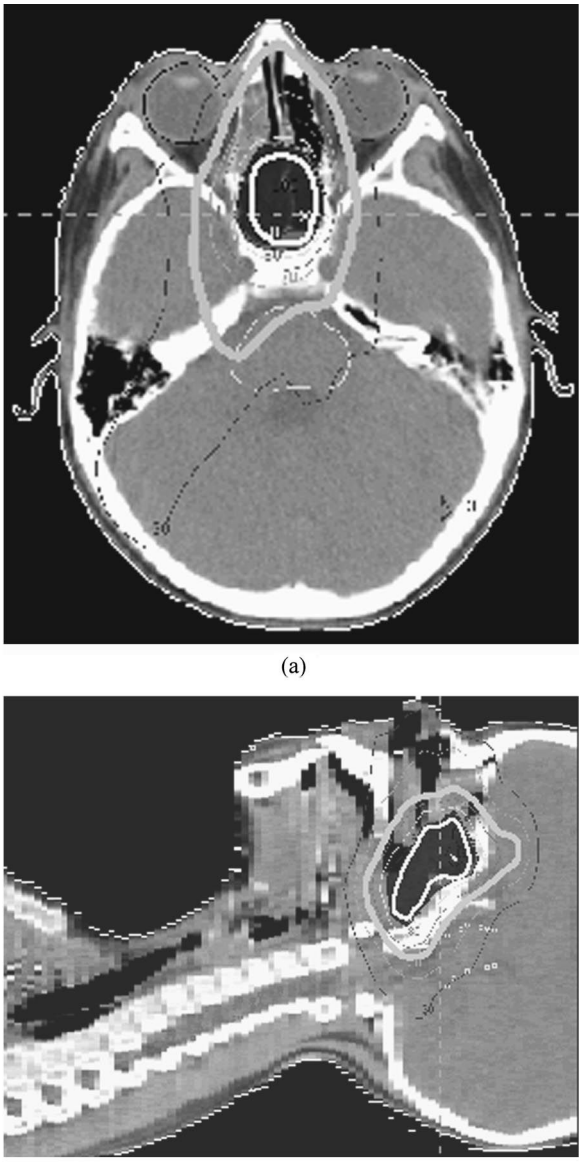

(a)

(b)

FIG. 12. An axial (a) and sagittal (b) image of the dose distribution for a head and neck patient. Seven beam angles are used with three apertures per beam angle. The tumor volume is outlined in white and the dark dose-cloud shows the 95% isodose coverage. The 50% isodose line is plotted as a thick gray line.

schedule was used and each optimization was terminated after 10 000 successful iterations. The extent to which local minima are affecting the quality of the final solution should be reflected in the degree of variation among these plans.

J. Comparison with a commercial inverse-planning system

The first phantom case and the head and neck patient were each optimized using a commercial inverse-planning system (CORVUS, Nomos Corporation, Sewickly, PA). CORVUS makes use of the traditional two-step approach to inverse planning in which an optimized pencil beam intensity pattern is translated into a set of deliverable apertures. This comparison is designed to illustrate the extent to which DAO can match the quality of dose distribution produced by the conventional two-step approach to IMRT. The comparison also serves to illustrate the extent to which DAO can reduce the number of segments and the required number of monitor units to deliver a step-and-shoot plan.

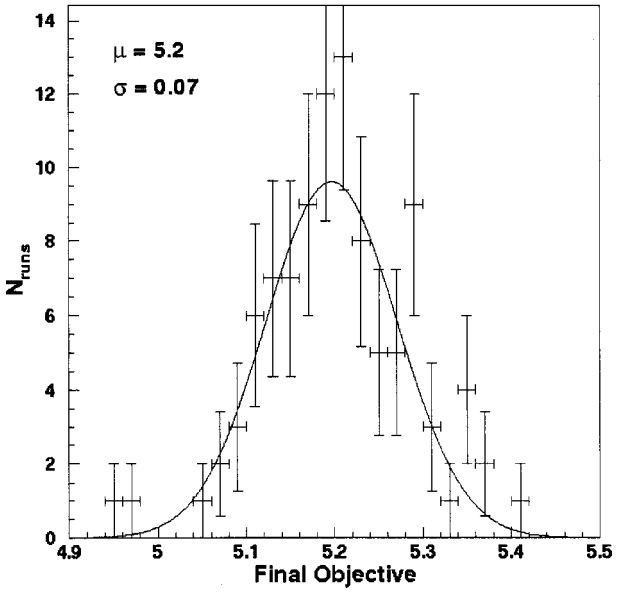

FIG. 13. An optimization was run 100 times with different random number seeds. This plot shows the results of fitting the histogram of final objective functions to a Gaussian. The error bars are stastical.

III. RESULTS

A. Phantom results

In Fig. 5, the optimized dose distribution and the corresponding DVH are shown for the cylindrical phantom with a concave target and an adjacent sensitive structure. Seven equispaced beam angles were used with three apertures per angle. Note that the 90% isodose line conforms tightly to the boundary of the tumor volume. This optimization was performed in 3.35 min on a 1.2 GHz PC running LINUX.

Prior to the optimization, it was specified that the optimization would stop after 4000 successful iterations. An iteration is considered successful if a change results in either a decrease in the objective function value or an increase in the objective function value that passes the probability constraint. In Fig. 6, the objective function value for this case is plotted versus the iteration number. The change in objective function is less than 1% after 2000 iterations. Figure 6 plots both the current objective function value and the best objective function value. These two curves are not identical, because the simulated annealing algorithm will accept some changes that increase the objective function's value. At the end of the optimization, the optimizer outputs those settings that provided the best objective function value.

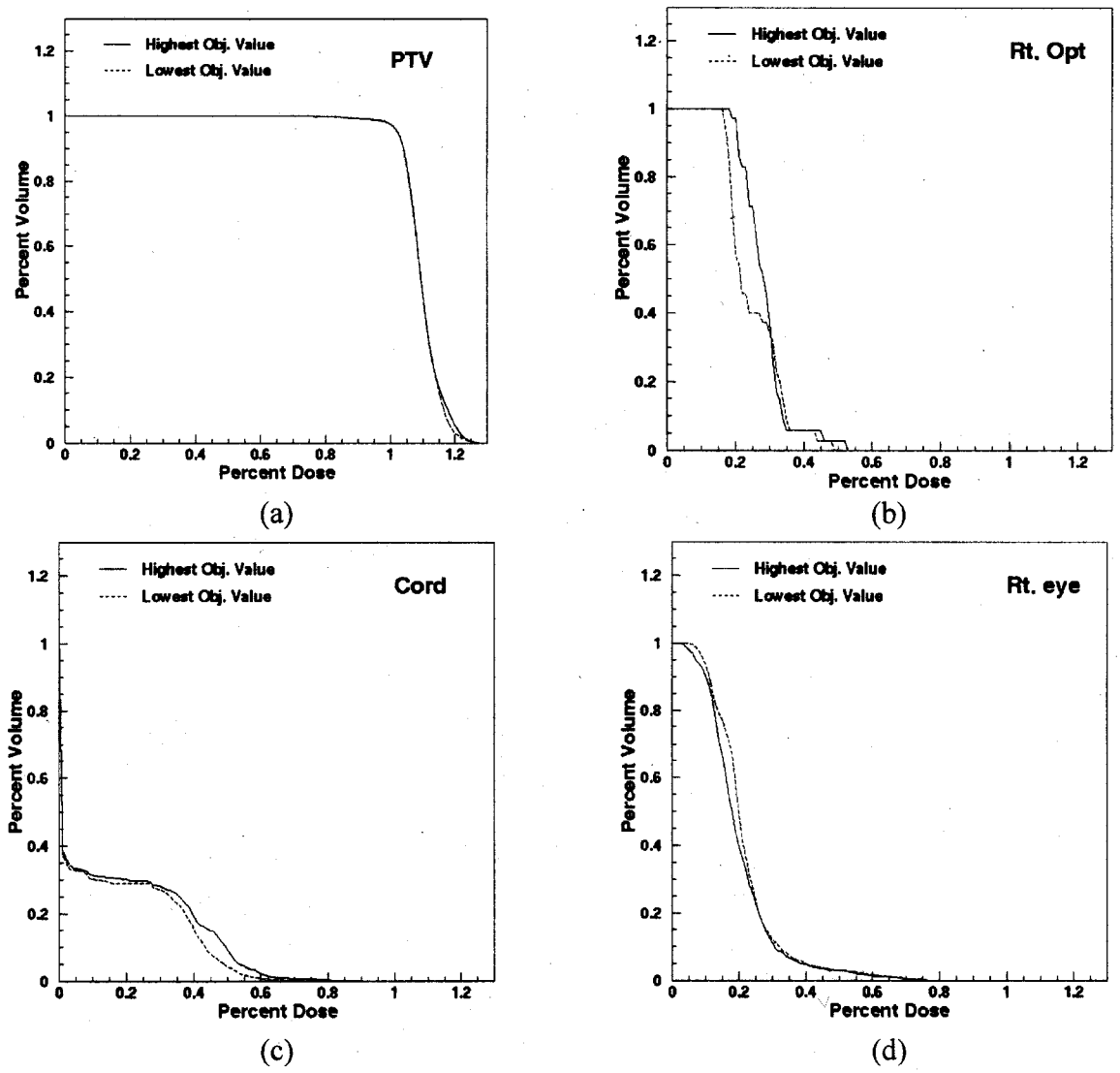

FIG. 14. The resulting dose volume histograms for the best and worst results obtained from 100 separate optimizations. Note that only modest differences are seen in the DVHs.

We should note that the required number of iterations varies depending upon both the complexity and size the target shape along with the number of variables included in the optimization. Although we choose to use the number of successes as our termination criteria, any of a number of other means could be used to specify the termination point.

In Fig. 7, the aperture shapes for one beam direction are shown along with the corresponding intensity map. Each shape meets the constraints imposed by the Elekta MLC. Note that in combination, the three apertures produce six nonzero beam intensities from this beam angle.

The accuracy of delivery with DAO has been validated using our cylindrical phantom. Figure 8 shows a comparison between predicted and measured results. This plan was delivered in approximately 7 min on an Elekta SL20 linear accelerator. In comparing the measured and predicted dose distributions, the 95% isodose lines agreed within 3 mm.

For the C-shaped target shown in Fig. 9, the DAO algorithm was run using 1, 3, 5, 7, and 9 apertures per beam direction. This test was designed to examine the extent to which the quality of a plan is related to the number of apertures. The pronounced nature of the concavity in this case makes it very difficult to simultaneously obtain a uniform target dose and significant sparing of the sensitive structure. Figure 9 shows the dose distribution obtained using seven apertures.

The final objective function for each of these optimizations is provided in Table I. With each increase in the number of apertures, the optimizer is provided with a corresponding increase in flexibility. Consequently, the final objective function value decreased with each increase in the number of apertures per beam direction. The results are compared in a DVH format in Fig. 10. Table I also lists the optimization time for each run. Note that the optimization time increases as the number of apertures increase. This is related to the increase in the number of variables that need to be optimized.

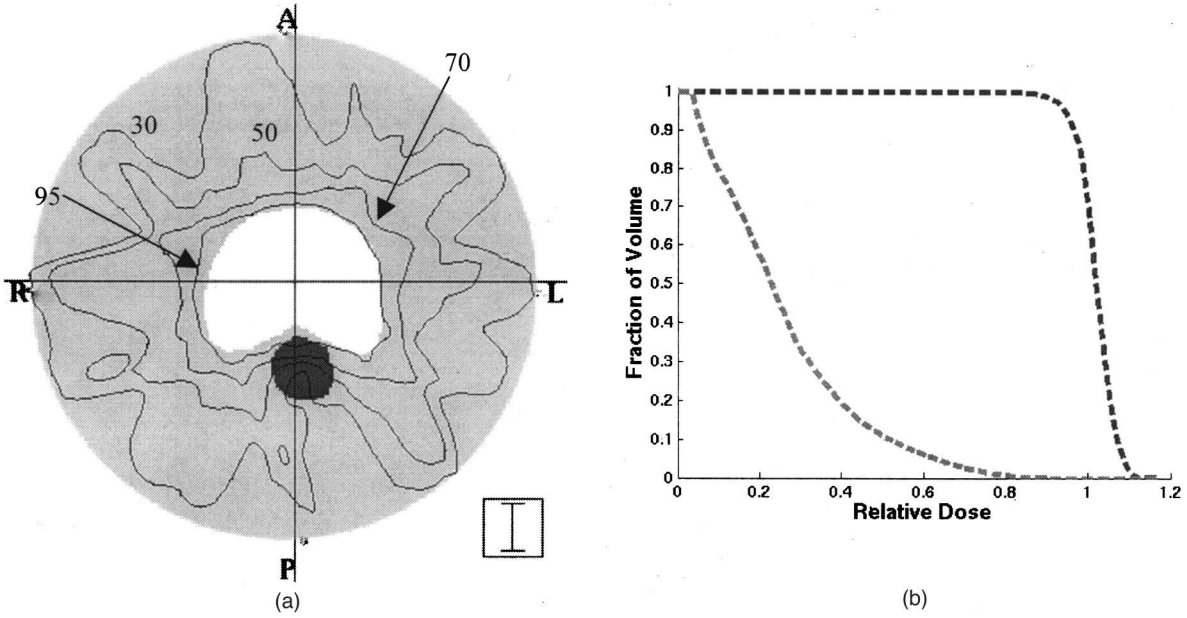

FIG. 15. Results produced by CORVUS for the same setup shown in Fig. 5. (a) The optimized dose distribution for seven beam angles with three intensity levels per beam direction. (b) The corresponding DVH.

B. Prostate patient

In Fig. 11, results are shown from the application of DAO to a patient with prostate cancer. A conformal dose distribution has been produced using seven equispaced beam angles and three apertures per angle. This optimization was performed in 5 min on a 1.2 GHz PC.

C. Head and neck results

In Fig. 12, isodose distributions are shown for a sagittal and an axial slice for a head and neck case optimized using DAO. Seven beam angles were used with three apertures per beam angle. This case is particularly difficult due to the proximity of the eyes, the optic nerves, and the brainstem.

D. Result of consistency test

For the head and neck case described above, 100 separate optimizations were performed with a different random number seed used in each case. In all cases, three apertures per beam direction were used along with the same prescription parameters. Each optimization was terminated after 10 000 successful iterations, and the optimization times varied between 6 and 7 min. The resulting histogram of final objective function values was fit to a Gaussian distribution. The results are plotted in Fig. 13. The resulting fit parameters are a mean of 5.2 and a standard deviation of 0.07. The minimum objective function value from the 100 runs was 4.95 and the maximum value was 5.41. For these two extremes, the resulting dose volume histograms are plotted in Fig. 14. Note that only modest differences in the DVHs are seen. If a slower cooling schedule was used in combination with a longer optimization time, these differences could be further minimized. We are, however, satisfied that the schedule that we are using strikes an appropriate balance between the need for a short optimization and the need to avoid local minima.

E. Comparison with CORVUS

For the first phantom case, a treatment plan was optimized using CORVUS with the identical beam arrangement as that applied using the DAO approach. The optimized dose distribution and corresponding DVH are plotted in Fig. 15. A DVH comparison between DAO and CORVUS (see Fig. 16) demonstrates that similar dosimetric results were obtained. In the phantom case, the DAO plan included a total of 21 apertures as compared with 144 apertures in the CORVUS plan, an 85% reduction in the number of apertures. The DAO plan required 500 monitor units to deliver the prescribed dose of 200 cGy. This is a 74% reduction as compared to the CORVUS plan, which used 1860 monitor units in order to deliver the same dose. If both plans could be delivered with 400 MU/min machine dose rate, the beam on time for delivering the CORVUS plan and the DAO plan would be 4.25 min and 1.25 min, respectively. However, a more dramatic difference is seen on linear accelerators that require an intersegment delay time. For a seven second intersegment delay, the total delay time between segments would amount to 16.8 min for the CORVUS plan as compared with 2.45 min with the DAO plan. Table II outlines the comparison between the two systems.

In Fig. 17 a DVH comparison is provided between DAO and CORVUS for the head and neck patient. This patient had previously been treated in our clinic using the CORVUS plan. The same seven beam angles were used in each case. In comparing the dose volume histograms, it can be seen

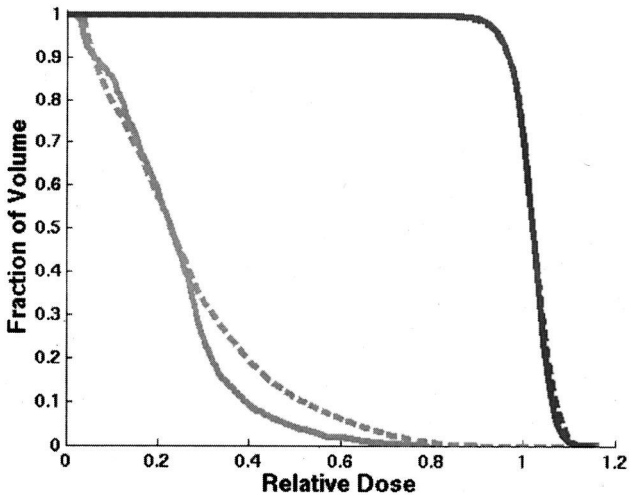

FIG. 16. A DVH comparison of the results produced by direct aperture optimization (solid lines) and the corresponding results produced by CORVUS (dashed lines).

that the plan produced using DAO provided improved tumor dose homogeneity as compared with CORVUS. The CORVUS plan, however, provided improved sparing of the critical structures. By adjusting the relative weights assigned to the treatment goals, it may be possible to further reduce the differences between these two plans.

TABLE II. A comparison of two treatment plans produced for a phantom study, one produced with direct aperture optimization, and one produced using CORVUS. In both cases, the same setup and same treatment goals were used. Note that DAO leads to a 85% reduction in the number of segments and a 74% reduction in the total number of monitor units.

	Direct aperture optimization	CORVUS
Total No. of segments	21	144
Total No. of monitor units	500	1860

Table III provides a comparison in terms of the number of segments and the total number of monitor units. The CORVUS plan used 221 segments as compared to 21 for the DAO plan. The CORVUS plan used 1761 MU as compared with 338 MU with the DAO plan.

It should be emphasized that these results are specific to the use of CORVUS in conjunction with an Elekta MLC. It is possible that with improved leaf sequencing[23,24] or smoothing of the intensity maps,[25] one could reduce the number of segments associated with the conventional two-step approach.

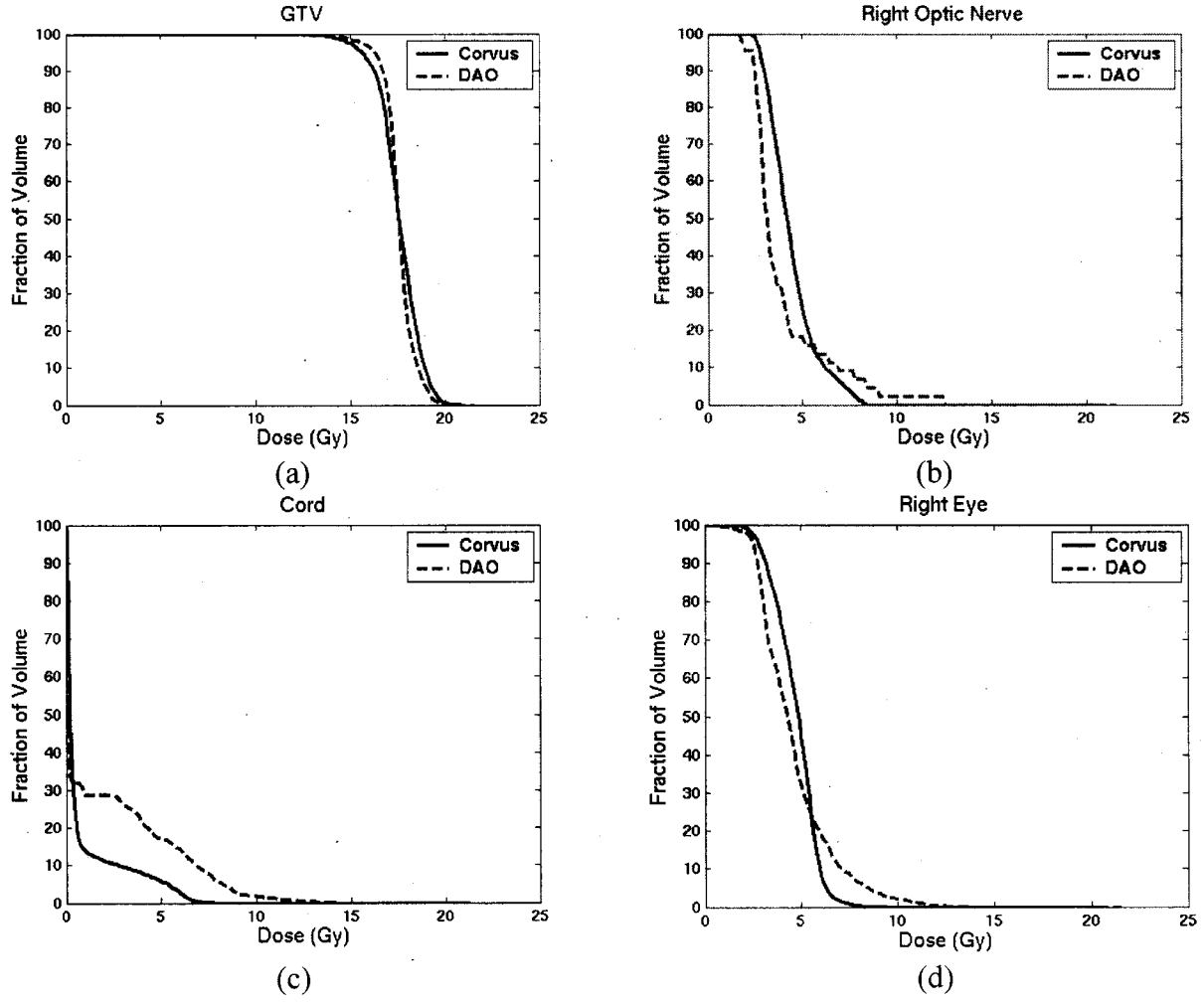

FIG. 17. A DVH comparison with CORVUS for the head and neck patient.

TABLE III. A comparison of two treatment plans for a head and neck patient, one produced with direct aperture optimization, and one produced using CORVUS. In both cases, the same setup beam arrangement and treatment goals were used.

	Direct apertureoptimization	CORVUS
Total No. of segments	21	221
Total No. of monitor units	338	1761

Comparing CORVUS with DAO, the impact of leakage and the tongue and groove effect would be more pronounced with CORVUS due to the large number of beam segments. In addition, the influence of patient motion would be increased due to the use of beam segments that are small in size.[1] Both of these considerations decrease the accuracy of the dose delivery.

IV. DISCUSSION

As compared with conventional IMRT planning techniques, DAO is able to produce comparable dose conformity with more efficient treatment deliveries. The reduction in the number of beam segments not only improves delivery efficiency, it also makes it easier to perform the required quality assurance (QA) procedures. Concerns regarding the dosimetric effects associated with current IMRT delivery, such as the use of small MUs, tongue and grove effects, and head scatter uncertainties for very small off-axis fields, are greatly reduced.

Another benefit of this technique is that the user is given considerable control over the complexity of the treatment plan. For instance, if the user prescribes one aperture per beam direction, a 3D conformal plan is produced; if the user prescribes five or six apertures per beam direction, a highly modulated IMRT plan can be produced. With this technique, one can take an incremental approach to the implementation of IMRT by starting with two apertures per beam direction and gradually increasing to five or six.

Another important feature of this tool is the flexibility of simulated annealing algorithm. One can easily replace the least squares objective function, which is based on the physical dose distribution with a biological objective function such as the equivalent uniform dose, TCP, or P+.[26–32] Due to their highly nonlinear nature, biological objective can be difficult to implement into other mathematical programming formulations in a robust fashion.

DAO can also be applied to the optimization of intensity modulated arc therapy (IMAT).[33] With IMAT optimization, one can specify the maximum number of arcs as input to the optimizer. Additional constraints need to be added to ensure that changes in the aperture shape from one beam angle to the next do not violate constraints on the maximum leaf velocity. Our IMAT results will be presented in a future publication. We will also present results showing how this technique can be used to produce hybrid plans that combine rotational and fixed field IMRT.[34]

V. CONCLUSIONS

We have developed an IMRT inverse planning strategy using direct aperture optimization. The MLC constraints are incorporated into the optimization algorithm, therefore eliminating the need for leaf sequencing. Results show that highly conformal IMRT treatment plans can typically be produced using five or fewer apertures per beam direction. This tool improves both the efficiency and the accuracy of IMRT delivery.

ACKNOWLEDGMENTS

This research was partially supported by National Science Foundation Grant No. ACI-0113051 and by National Institute of Health Grant No. R29CH66075. The authors would like to thank Timothy Holmes for his contribution to this work. Finally, the authors thank Mark Symons, Peter Maton, and Rajesh Raut of Elekta for their assistance.

[1] T. Bortfeld, D. H. Haler, T. J. Waldron, and A. L. Boyer, "X-ray compensation with multileaf collimators," Int. J. Radiat. Oncol., Biol., Phys. **28**, 723–739 (1994).
[2] C. S. Chui, T. LoSasso, and S. Spirou, "Dose calculation for photon beam with intensity modulation generated by dynamic jaw or multileaf collimation," Med. Phys. **21**, 1237–1244 (1994).
[3] J. M. Galvin, X. G. Chen, and R. M. Smith, "Combining multileaf field to modulate fluence distributions," Int. J. Radiat. Oncol., Biol., Phys. **27**, 697–705 (1993).
[4] S. Webb, "Optimizing the planning of intensity-modulated radiotherapy," Phys. Med. Biol. **39**(12), 2229–2246 (1994).
[5] S. Webb, "Configuration options for intensity-modulated radiation therapy using multiple static fields shaped by a multileaf collimator," Phys. Med. Biol. **43**(2), 241–260 (1998).
[6] S. Webb, "Configuration options for intensity-modulated radiation therapy using multiple static fields shaped by a multileaf collimator. II: Constraints and limitations on 2D modulation," Phys. Med. Biol. **43**(6), 1481–1495 (1998).
[7] P. Xia and L. J. Verhey, "Mutileaf collimation leaf sequencing algorithm for intensity modulated beams with multiple static segments," Med. Phys. **25**, 1424–1434 (1998).
[8] J. Tervo and P. Kolmonen, "A model for the control of a multileaf collimator in radiation therapy treatment planning," Inverse Probl. **16**, 1875–1895 (2000).
[9] W. DeGersem, F. Claus, C. DeWagter, B. VanDuyse, and W. DeNeve, "Leaf position optimization for step-and-shoot IMRT," Int. J. Radiat. Oncol., Biol., Phys. **51**(5), 1371–1388 (2001).
[10] R. Rardin, *Optimization in Operations Research* (Prentice Hall, Englewood Cliffs, NJ, 1998).
[11] S. Kirkpatrick, C. D. Gelatt, Jr., and M. P. Vecchi, "Optimization by simulated annealing," Science **220**(4598), 671–680 (1993).
[12] S. Geman and D. Geman, "Stochastic relaxation, Gibbs distribution and the Bayesian restoration in images," IEEE Trans. Pattern Anal. Mach. Intell. **6**(6), 731–741 (1984).
[13] M. Pincus, "A Monte Carlo Method for the approximate calculation of certain types of constrained optimization problems," Oper. Res. **18**, 1225–1228 (1970).
[14] V. Cerny, "A thermodynamic approach to the traveling salesman problem: An efficient simulation algorithm," Report, Comenius University, Brathislava, Czechoslovakia, 1982.
[15] K. Binder and D. Stauffer, "A simple introduction to Monte Carlo simulations and some specialized topics," in *Statistical Physics*, edited by K. Binder (Springer-Verlag, Berlin, 1985), pp. 1–36.
[16] T. J. Jordan and P. C. Williams, "The design and performance characteristics of a multileaf collimator," Phys. Med. Biol. **39**, 231–251 (1994).
[17] *Multileaf Collimator (MLC) Operator's Manual for MLC SA1*, Philips Medical Systems, Document No. 4522 984 40891/764, Appendix C, 1993.

[18] T. Bortfeld, J. Stein, and K. Preiser, "Clinically Relevant Intensity Modulation Optimization Using Physical Criteria," in Proceeding of the XII International Conference on the Use of Computers in Radiation Therapy, Salt Lake City, UT (1997).
[19] D. M. Shepard, G. H. Olivera, P. J. Reckwerdt, and T. R. Mackie, "Iterative approaches to dose optimization", Phys. Med. Biol. **45**, 69–90 (1999).
[20] Chapter 15: "Tomotherapy," *The Modern Technology of Radiation Oncology, a Compendium for Medical Physicists and Radiation Oncologists*, edited by J. Van Dyck, G. H. Olivera, D. M. Shepard, K. Ruchala, J. S. Aldridge, J. Kapatoes, E. E. Fitchard, P. J. Reckwerdt, G. Fang, J. Balog, J. Zachman, and T. R. Mackie (Medical Physics, Madison, WI, 1999).
[21] D. W. O. Rogers, B. A. Faddegon, G. X. Ding, C. M. Ma, J. Wei, and T. R. Mackie, "BEAM: a Monte Carlo code to simulate radiotherapy treatment unit," Med. Phys. **22**, 503–524 (1995).
[22] X. A. Li, L. Ma, S. Naqvi, R. Shih, and C. Yu, "Monte Carlo dose verification for intensity modulated arc therapy," Phys. Med. Biol. **46**(9), 2269–2282 (2001).
[23] M. Langer, V. Thai, and L. Papiez, "Improved leaf sequencing reduces segments or monitor units needed to deliver IMRT using multileaf collimators," Med. Phys. **28**, 2450–2458 (2001).
[24] J. Dai and Y. Zhu, "Minimizing the number of segments in a delivery sequence for intensity-modulated radiation therapy with a multileaf collimator," Med. Phys. **28**, 2113–2120 (2001).
[25] S. V. Spirou, N. Fournier-Bidoz, J. Yang, C. S. Chui, and C. C. Ling, "Smoothing intensity-modulated beam profiles to improve the efficiency of delivery," Med. Phys. **28**, 2105–2112 (2001).
[26] P. Stavrev, N. Stavreva, A. Niemierko, and M. Goitein, "Generalization of a model of tissue response to radiation based on the idea of functional subunits and binomial statistics," Phys. Med. Biol. **46**, 1501–1518 (2001).
[27] L. C. Jones and P. W. Hoban, "Treatment plan comparison using equivalent uniform biologically effective dose (EUBED)," Phys. Med. Biol. **45**(1), 159–170 (2000).
[28] A. Niemierko, "Radiobiological models of tissue response to radiation in treatment planning systems," Tumori **84**(2), 140–143 (1998).
[29] A. Niemierko, "Reporting and analyzing dose distributions: a concept of equivalent uniform dose," Med. Phys. **24**, 103–110 (1997).
[30] A. Brahme, "Individualizing cancer treatment: biological optimization models in treatment planning and delivery" Int. J. Radiat. Oncol., Biol., Phys. **49**(2), 327–337 (2001).
[31] A. Brahme, "Biologically based treatment planning," Acta Oncol. **38**(Suppl. 13), 61–68 (1999).
[32] A. Brahme, "Optimized radiation therapy based on radiobiological objectives," Semin. Radiat. Oncol. **9**(1), 35–47 (1999).
[33] M. A. Earl, D. M. Shepard, X. A. Li, and C. X. Yu, "Inverse planning for intensity modulated arc therapy using direct aperture optimization," Int. J. Radiat. Oncol., Biol., Phys. **51**(3), Suppl. 1, 404 (2001).
[34] C. X. Yu and J. Li, "Angular Cost—A new concept for broad-scope planning optimization," Int. J. Radiat. Oncol., Biol., Phys. **51**(3), Suppl. 1, 406 (2001).